Gas-Phase Reactions of the Iodide Ion with Chloromethane and Bromomethane: Competition between Nucleophilic Displacement and Halogen Abstraction†

Laurence A. Angel and Kent M. Ervin*

Department of Chemistry and Chemical Physics Program, University of Nevada, Reno, 1664 North Virginia Street, Reno, Nevada 89557

Received: March 30, 2004; In Final Form: May 29, 2004

Guided ion beam tandem mass spectrometry techniques are used to measure the reaction cross sections of the collisionally activated process $I^- + CH_3Y \rightarrow$ products, where Y = Cl and Br. The Cl^- and Br^- products are observed at the lowest collision energies. A back-side attack S_N2 reaction is responsible for the initial rise from the threshold. At higher collision energies, the ICl^- and IBr^- ions are observed and signify competition from a front-side-attack, halogen-abstraction reaction. All the reactions are endoergic and exhibit excess threshold energies, E_0, when compared with established reaction endothermicities from the literature, ΔH_0. The reaction mechanisms are explored with the aid of CCSD(T)/LanL2DZ and CCSD(T)/SDD molecular orbital calculations and phase space theory.

1. Introduction

The study of ion−molecule reactions in the gas phase provides the opportunity to investigate the intrinsic reaction mechanism in isolation from solvent. One of the most studied ion−molecule reactions is the bimolecular nucleophilic substitution (S_N2) reaction,[1−5] which proceeds through a double-well potential energy surface (PES)[6−8] concurrent with a back-side attack mechanism accompanied by inversion of the methyl group. Gas-phase $X^- + CH_3Y$ S_N2 reactions have shown an inherent inefficiency explained by dynamical constraints.[4,9−15] For example, the threshold energies of the endothermic $Cl^- + CH_3F$ reaction exhibited excess threshold energies to the reaction endothermicity.[16] The validity of statistical theories such as Rice−Ramsperger−Kassel−Marcus theory and phase space theory (PST) in modeling the gas-phase S_N2 reaction have also been called into question.[4,10,11,17−23] Most of the previous gas-phase S_N2 studies[1] have investigated exothermic reactions at or near thermal temperatures. The guided ion beam tandem mass spectrometry (GIB-MS) technique, in comparison, allows for a wide range of collision energies between the halide ion and halomethane to be explored. Previous GIB-MS studies have also observed alternative reactions such as halogen abstraction (a front-side attack mechanism), proton transfer, and hydrogen halide elimination.[16,24−27] This work investigates whether S_N2 reactions containing heavier halogens than previously studied behave statistically and whether the threshold energies match the thermochemical endothermicities.

In the present study, we present the energy-dependent cross sections of the endoergic reactions of $I^- + CH_3Y$, where Y = Cl or Br, using GIB-MS. To our knowledge, there have only been two previous reports of endoergic reactions of $X^- + CH_3Y$, where both X and Y are halogens. The work of Zellermann and Vietzke[28] used an ion beam/gas cell technique to measure the collision energy dependence of the products H^-, F^-, FBr^-, and CH_2Br^- from the reaction $Br^- + CH_3F$ and of products F^-, FI^-, and CH_2I^- from $I^- + CH_3F$. Our group reported[16] the collision-energy-dependent cross sections for the products F^-, FCl^-, CH_2Cl^-, and $CHCl^-$ from the reaction $Cl^- + CH_3F$.

The endothermic reactions 1 and 2 can be driven by translational energy, where Y = Cl or Br.

$$I^- + CH_3Y \rightarrow Y^- + [CH_3I] \quad (1)$$

$$I^- + CH_3Y \rightarrow IY^- + [CH_3] \quad (2)$$

Reaction 1 represents the conventional S_N2 back-side attack reaction at low energies where the CH_3I stays intact. However, at the higher collision energies investigated here, Y^- may also be accompanied by the fragmentation of CH_3I or proceed by a front-side Y^- displacement mechanism. Reaction 2 represents the halogen abstraction reaction at the energies where an alternative front-side attack reaction can compete. The simultaneous detection of reactions analogous to 1 and 2 has been previously reported in halide/halomethane systems: the Br^- and $ClBr^-$ ions from the reaction $Cl^- + CH_3Br$,[24,27] Cl^- and Cl_2^- from $Cl^- + CH_3Cl$,[25] and F^- or Cl^- with FCl^- from $Cl^- + CH_3F$ and $F^- + CH_3Cl$.[16,26] The dynamics and competition among reactions 1 or 2 are discussed here with the aid of PST and molecular orbital calculations at the CCSD(T)/LanL2DZ and CCSD(T)/SDD levels of theory.

2. Experimental Methods

Iodide anions are produced in a microwave discharge source from the vapor of iodine crystals added in trace amounts into a flowing buffer gas of helium. The I^- anions pass along a flow tube and are sampled through a nose cone into the guided ion beam tandem mass spectrometer.[25] A series of lenses shapes, focuses, and accelerates the anions to a magnetic mass spectrometer, which mass selects $^{127}I^-$ before injection into an octopole radio frequency ion beam guide. Situated at the center of the octopole is a reaction cell where the chloromethane or bromomethane reactant gas is introduced. The collision energy between the iodide ions and the neutral gas is controlled by the direct current (dc) potential difference between the flow tube ion source and the octopole. The anionic reactants and products

† Part of the special issue "Tomas Baer Festschrift".

* Corresponding author. E-mail: ervin@chem.unr.edu.

10.1021/jp048605v CCC: $27.50
Published on Web 07/16/2004

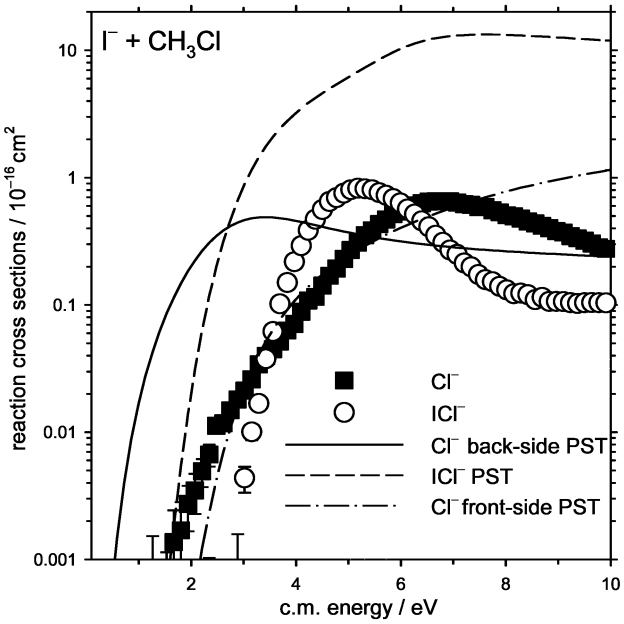

Figure 1. Experimental cross sections (symbols) for the product ions Cl^- and ICl^- from the reaction of $I^- + CH_3Cl$ as a function of relative collision energy in the center-of-mass frame. PST cross sections (lines) for back-side and front-side nucleophilic displacement and the front-side halogen abstraction mechanism are also shown.

are then extracted from the octopole and injected into a quadrupole mass spectrometer where they are mass analyzed. Ion intensities are detected by a collision dynode/channeltron multiplier operated in negative-ion pulse counting mode.

Absolute reaction cross sections are determined as a function of collision energy by scanning the octopole dc potential and counting the reactant and product ions for predetermined dwell times.[25] The laboratory ion energy is measured using retarding potential analysis, confirmed by time-of-flight measurements, and converted to relative collision energy, E, in the center-of-mass frame.[25,29] Background ion counts from reactions occurring outside the reaction cell are also collected and subtracted from the total. All cross sections are measured at three pressures in the range $(5-20) \times 10^{-5}$ mbar. The results are extrapolated to zero pressure by a least-squares linear regression, ensuring that the reported cross sections are in the single-collision limit.[25,29]

The threshold behavior of the cross section, $\sigma(E)$, is modeled by using an empirical threshold law,[25,29−32]

$$\sigma(E) = \sigma_0 \sum_i g_i[E + E_i - E_0]^N/E \qquad (3)$$

where E_i is the internal energy of reactant state i with fractional thermal population g_i corresponding to a Boltzmann distribution at 300 K, σ_0 and N are adjustable parameters, and E_0 is the 0 K reaction threshold energy. Experimental[33] vibrational frequencies and rotational constants of CH_3Y are used for the sum over the reactant internal energy density of states.[31,32] Finally, eq 3 is convoluted over the experimental collision energy distributions[34,35] as described previously.[29] The reported error limits represent ±2 combined standard uncertainties[36] or an approximate 95% confidence level. These calculations are performed using the CRUNCH data analysis program.[37] Classical PST cross sections[38−40] are also calculated with CRUNCH. The ab initio calculations described in the following were performed using the Gaussian 98 suite of programs.[41]

TABLE 1: Threshold Energies and Enthalpies for the Reaction $I^- + CH_3Cl \rightarrow$ Products (kJ mol^{-1})

reaction	product ion	E_0 (this work)	possible contributing reaction	ΔH_0 (lit.)[a]
$I^- + CH_3Cl$	Cl^-	134 ± 31	$Cl^- + CH_3I$	57 ± 1
			$Cl^- + I + CH_3$	290 ± 1
			$Cl^- + I + CH + H_2$	734 ± 1
			$Cl^- + I + CH_2 + H$	747 ± 4
$I^- + CH_3Cl$	ICl^-	352 ± 28	$ICl^- + CH_3$	197 ± 10[b]
			$ICl^- + CH + H_2$	641 ± 10[b]
			$ICl^- + CH_2 + H$	653 ± 10[b]

[a] Enthalpies of reactions calculated with enthalpies of formation values cited in Gurvich et al.[42,43] except as noted. [b] Enthalpy of formation of ICl^- from NIST database.[60]

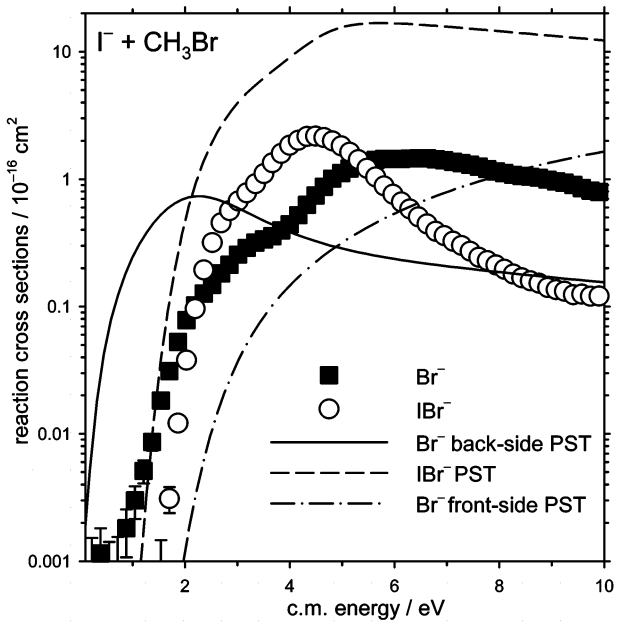

Figure 2. Experimental cross sections (symbols) for the product ions Br^- and IBr^- from the reaction of $I^- + CH_3Br$ as a function of relative collision energy in the center-of-mass frame. PST cross sections (lines) for back-side and front-side nucleophilic displacement and the front-side halogen abstraction mechanism are also shown.

3. Results

3.1. Cross Sections for $I^- + CH_3Cl$. The experimental reaction cross sections from 0.1 to 10 eV are shown in Figure 1. Two products ions, Cl^- and ICl^-, are observed. Table 1 compares the threshold energies, obtained by fits of eq 3 to the rising cross sections, with literature thermochemical values.[42,43] The Cl^- cross sections exhibit a threshold energy of $E_0 = 1.39 \pm 0.32$ eV (134 ± 31 kJ/mol) and rise to 0.65×10^{-16} cm^2 by 6 eV, before declining at higher energies. The ICl^- cross sections rise from a threshold energy of $E_0 = 3.65 \pm 0.29$ eV (352 ± 28 kJ/mol) to a cross section of 0.82×10^{-16} cm^2 by 5 eV and decline at higher energies.

3.2. Cross Sections for $I^- + CH_3Br$. The reaction cross sections of Br^- and IBr^- from 0.1 to 10 eV are shown in Figure 2. Table 2 compares the measured threshold energies with the literature thermochemical values.[42,43] The formation of Br^- exhibits a threshold of $E_0 = 1.25 \pm 0.10$ eV (121 ± 10 kJ/mol) with the cross sections rising to a maximum 1.5×10^{-16} cm^2 by 6 eV, before showing a decline at higher energies. The formation of IBr^- exhibits a threshold energy of $E_0 = 2.23 \pm 0.21$ eV (215 ± 20 kJ/mol) with the cross sections rising to 2.2×10^{-16} cm^2 by 4 eV, before declining at higher energies.

3.3. Molecular Orbital Calculations. CCSD(T)/LanL2DZ and CCSD(T)/SDD geometry optimization and frequency

TABLE 2: Threshold Energies and Enthalpies for the Reaction $I^- + CH_3Br \rightarrow$ Products (kJ mol^{-1})

reaction	product ion	E_0 (this work)	possible contributing reaction	ΔH_0 (lit.)[a]
$I^- + CH_3Br$	Br^-	121 ± 10	$Br^- + CH_3I$	27 ± 1
			$Br^- + I + CH_3$	260 ± 1
			$Br^- + I + CH + H_2$	704 ± 1
			$Br^- + I + CH_2 + H$	716 ± 4
$I^- + CH_3Br$	IBr^-	215 ± 20	$IBr^- + CH_3$	154 ± 10[b]
			$IBr^- + CH + H_2$	599 ± 10[b]
			$IBr^- + CH_2 + H$	611 ± 10[b]

[a] Enthalpies of reactions calculated with enthalpies of formation values cited in Gurvich et al.[42,43] except as noted. [b] Enthalpy of formation of IBr^- from NIST database.[60]

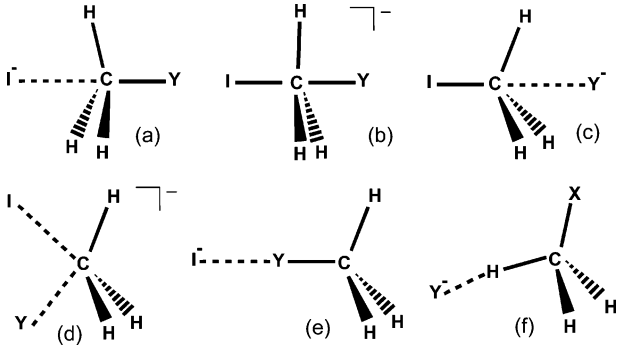

Figure 3. (**a**) Entrance S_N2 ion−dipole complex, (**b**) S_N2 transition state, (**c**) exit S_N2 ion−dipole complex, (**d**) front-side nucleophilic exchange transition state, (**e**) halogen-bonded complex, (**f**) halogen hydrogen-bonded complex.

calculations were performed using Gaussian 98[41] to calculate the 0 K energies of possible stationary points for reactions 1 and 2. The LanL2DZ basis set includes the Dunning/Huzinaga full double-ζ basis set D95 for H and C,[44] and Los Alamos effective core potentials plus double-ζ for Cl, Br, and I.[45] The SDD basis set incorporates the valence double-ζ basis set D95V for H, C, and Cl[44] and Stuttgart/Dresden electron core potentials for Br and I.[46] The six structures illustrated in Figure 3 are investigated. The top three structures **a**−**c** are the back-side attack S_N2 intermediates. Tables 3 and 4 compare the CCSD(T)/LanL2DZ and CCSD(T)/SDD S_N2 stationary points with previously reported G2(+) calculations by Radom and coworkers.[47] For the CCSD(T)/LanL2DZ theory, the energies of the ion−dipole complexes, for both S_N2 reactions, are all within 7 kJ/mol of the G2(+) energies. Both the transition states, however, are lower than the G2(+) energies, by 26 kJ/mol for $I^- + CH_3Cl$ and 18 kJ/mol for $I^- + CH_3Br$. Comparison of the final energy of the products with the experimental S_N2 reaction endothermicity, ΔH_0 listed in Tables 1and 2, shows CCSD(T)/LanL2DZ theory is within 4 kJ/mol while G2(+) theory is within 7 kJ/mol.

The CCSD(T)/SDD theory compares well with G2(+) for three of the ion−dipole complexes and one of the transition states, with energies all within 5 kJ/mol. There is poor agreement with the exit ion−dipole complex for the $I^- + CH_3Cl$ reaction (29 kJ/mol higher) and the transition state for $I^- + CH_3Br$ (10 kJ/mol lower). The CCSD(T)/SDD theory also gives S_N2 reaction endothermicities, ΔH_0, that compare poorly with the experimental values, 35 kJ/mol higher for the $I^- + CH_3Cl$ reaction and 18 kJ/mol lower for $I^- + CH_3Br$.

Although the three different levels of theory do not exhibit convergence for all the S_N2 stationary points, there is enough qualitative agreement to use the CCSD(T)/LanL2DZ and CCSD(T)/SDD theories to roughly estimate the energies of alternative stationary points that might be important for reactions 1 and 2 (structures **d**−**f** in Figure 3). However, for further discussion of the back-side attack S_N2 mechanism we shall use the energies calculated by the G2(+) method.[47] The schematic PES's for the two S_N2 reactions, exhibiting the G2(+) relative energies of the five stationary points, are shown in Figure 4.

The CCSD(T)/LanL2DZ and CCSD(T)/SDD stationary point energies for the front-side nucleophilic exchange transition state, **d**, for the $I^- + CH_3Cl$ and $I^- + CH_3Br$ reactions are shown in Tables 3 and 4. For $I^- + CH_3Cl$, the transition state is 183−203 kJ/mol higher in energy than the reactants, whereas for $I^- + CH_3Br$ the transition state is 166−167 kJ/mol higher in energy than the reactants.

For the front-side halogen attack minimum, **e**, the chlorine-bonded structure from the $I^- + CH_3Cl$ reaction follows a minimum energy path back toward reactants for both the CCSD(T)/LanL2DZ and the CCSD(T)/SDD methods, consistent with a completely repulsive surface out to products. This is confirmed

TABLE 3: $I^- + CH_3Cl$ Stationary Point Energies (kJ mol^{-1})

stationary point	CCSD(T)/LanL2DZ[a]	CCSD(T)/SDD[a]	G2(+)[b]
$I^- + CH_3Cl$	0	0	0
a C_{3v} $I^-\cdots CH_3Cl$ ion−dipole complex	−40.3	−31.2	−34.4
b C_{3v} $[I-CH_3-Cl]^-$ transition state	10.2	35.9	36.1
c C_{3v} $IH_3C\cdots Cl^-$ ion−dipole complex	3.8	32.8	4.1
d C_s $[IClCH_3]^-$ transition state	182.7	202.9	
e C_{3v} $I^-\cdots ClCH_3$ chlorine-bonded complex	repulsive[c]	repulsive[c]	
$Cl^- + CH_3I$	60.5	92.0	49.9

[a] Energies at 0 K relative to $I^- + CH_3Cl$ reactants and corrected for zero-point energy. [b] Glukhovtsev et al.[47] [c] Starting with an ion−molecule complex, the calculation follows a minimum path back towards reactants consistent with a repulsive surface.

TABLE 4: $I^- + CH_3Br$ Stationary Point Energies (kJ mol^{-1})

stationary point	CCSD(T)/LanL2DZ[a]	CCSD(T)/SDD[a]	G2(+)[b]
$I^- + CH_3Br$	0	0	0
a C_{3v} $I^-\cdots CH_3Br$ ion−dipole complex	−37.6	−31.1	−36.3
b C_{3v} $[I-CH_3-Br]^-$ transition state	−2.3	5.2	15.6
c C_{3v} $IH_3C\cdots Br^-$ ion−dipole complex	−16.1	−23.1	−22.8
d C_s $[IBrCH_3]^-$ transition state	165.9	166.5	
e C_{3v} $I^-\cdots BrCH_3$ bromine-bonded complex	4.4	2.4	
e C_{3v} $I^-\cdots BrCH_3$ bromine-bonded transition state	8.0	6.7	
$Br^- + CH_3I$	29.8	9.2	17.9

[a] Energies at 0 K relative to $I^- + CH_3Br$ reactants and corrected for zero-point energy. [b] Glukhovtsev et al.[47]

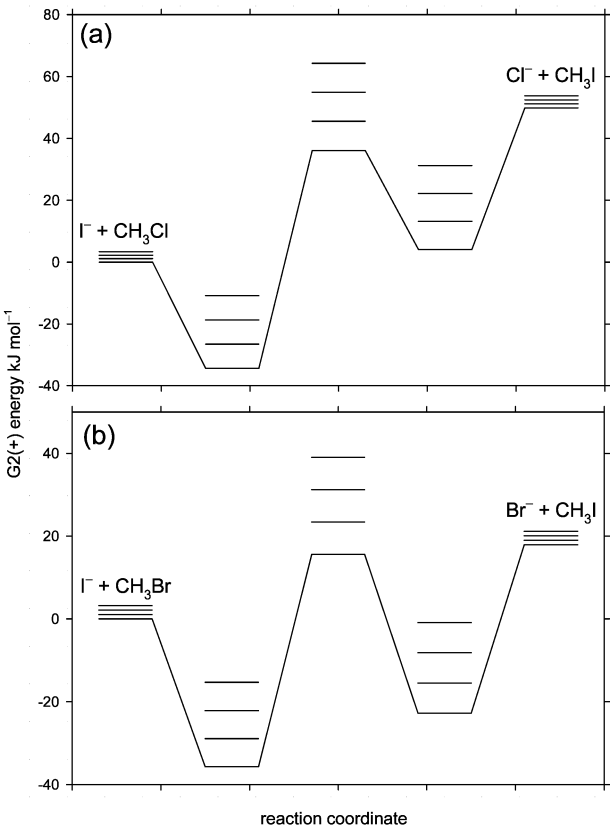

Figure 4. Schematic PES for (a) $I^- + CH_3Cl \rightarrow Cl^- + CH_3I$ and (b) $I^- + CH_3Br \rightarrow Br^- + CH_3I$ in C_{3v} symmetry calculated at the G2(+) level of theory.[47] Additional lines indicate the effective potentials with centrifugal terms at the stationary points for values of $Eb^2 = 200$, 400, and 600 (kJ/mol) Å^2. For the entrance and exit channels, the r(C−I) and r(C−Y) distances were held at 12 Å for the effective potentials.

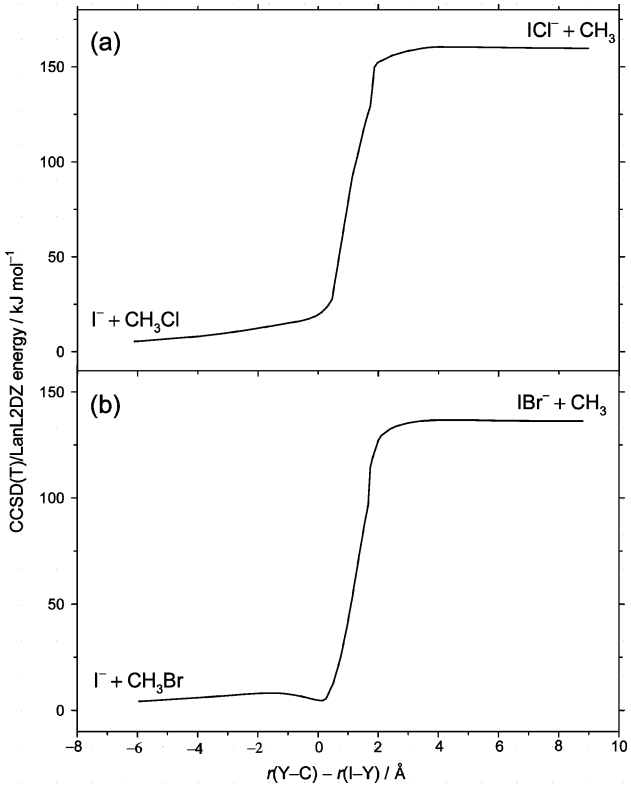

Figure 5. PES's for (a) $I^- + CH_3Cl \rightarrow ICl^- + CH_3$ and (b) $I^- + CH_3Br \rightarrow IBr^- + CH_3$ in C_{3v} symmetry calculated at the UCCSD(T)/LanL2DZ level of theory.

by the C_{3v} PES for the $I^- + CH_3Cl$ reaction calculated at the UCCSD(T)/LanL2DZ level and shown in Figure 5a. The unrestricted method is used for the PES of reaction 2 because the exit channel exhibits unpaired electrons in both product species. This type of PES has been previously observed by the $Cl^- + CH_3F \rightarrow FCl^- + CH_3$ reaction.[16] Table 4 shows that the bromine-bonded minimum structure, **e**, for the $I^- + CH_3Br$ reaction is 2−4 kJ/mol higher in energy than the reactants. The minimum structure is separated from the reactants by a transition state, **e**, that is 7−8 kJ/mol higher in energy than the reactants. The $I^- + CH_3Br \rightarrow IBr^- + CH_3$ PES in C_{3v} symmetry calculated at the UCCSD(T)/LanL2DZ level is shown in Figure 5b. The PES is similar to that for the $I^- + CH_3Cl$ system, except there is a shallow minimum in the entrance channel. This type of PES has been previously observed by the $F^- + CH_3Cl \rightarrow FCl^- + CH_3$ reaction.[26] At the top of the exit channels, there is an apparent maximum of about 1 kJ/mol higher in energy than the products. The exit channels shown in Figure 5 should be considered qualitative, however, because the unrestricted wave function exhibits a considerable amount of spin contamination and because of the restriction to C_{3v} symmetry.

Structure **f** was investigated as a possible hydrogen-bonded intermediate. In our previous work[16,26] on the $F^- + CH_3Cl$ and $Cl^- + CH_3F$ reactions, we detected the CH_2Cl^- ion. The fluoride ion has a hydrogen-bonding propensity that results in a hydrogen-bonded intermediate $F^-\cdots H-CH_2Cl$ 5 kJ/mol more stable than the ion−dipole complex $F^-\cdots CH_3Cl$.[16,26] Internal proton transfer from chloromethane to the fluoride ion results in the products $HF + CH_2Cl^-$. For the present systems with both CCSD(T)/LanL2DZ and CCSD(T)/SDD methods, we fail to locate minimum-energy hydrogen-bonded structures $Y^-\cdots H-CH_2X$, **f**, where X or Y = I, Cl, or Br. Instead, the geometries optimize to the ion−dipole $Y^-\cdots CH_3X$ structure **c**. This implies the ion−dipole complex is more stable than the hydrogen-bonded structure, unlike the fluoride ion case, and no significant potential energy barrier separates the two structures. Because of the qualitative nature of the energies at these levels of theory, no further attempts to locate transition states were made.

4. Discussion

4.1. $I^- + CH_3Cl \rightarrow Cl^- + [CH_3I]$. The ΔH_0 values listed in Table 1 show that the formation of Cl^- in the threshold region must be due to the $Cl^- + CH_3I$ products, because other channels have energies higher than the observed threshold. From the schematic PES for the S_N2 mechanism shown in Figure 4a, we can see that the central barrier on the PES (without any contribution from the centrifugal potential energy term) is lower in energy than the products. The Cl^- cross sections are a result of a back-side S_N2 mechanism, therefore, but the threshold energy, E_0, exhibits an excess of 77 ± 31 kJ/mol over the reaction endothermicity, ΔH_0. The excess threshold energy is not due to a potential energy barrier.

Table 3 shows the CCSD(T)/LanL2DZ and CCSD(T)/SDD energies for accessing a transition state for a front-side nucleophilic exchange mechanism, structure **d** in Figure 3. The methods give a transition state 183−203 kJ/mol above the energy of the reactants, which is too high to explain the observed reaction onset of 134 ± 31 kJ/mol. The excess threshold energy, therefore, is a result of dynamic constrictions rather than going over transition state **d**. Previously,[16] we observed similar excess thresholds for the endothermic S_N2 reaction of $Cl^- + CH_3F$ and discussed three effects that may contribute to the observed high threshold energy: angular momentum conservation, ori-

entational or steric constraints, and translational versus vibrational energy requirements. A brief discussion of these dynamical constrictions is included in section 4.5. At energies above 3 eV, the Cl^- cross sections may be augmented by a new front-side attack reaction mechanism passing through the transition state **d**. The reaction products $Cl^- + I + CH_3$ (Table 1) also become thermochemically viable and are related to the dissociation energy of ICl^- and the chlorine abstraction reaction discussed next.

4.2. $I^- + CH_3Cl \rightarrow ICl^- + [CH_3]$. Table 1 shows that the ICl^- cross sections at the threshold energy must be associated with the neutral product CH_3. The reaction is presumably a direct, front-side attack mechanism at the chlorine side (halophilic attack) of the CH_3Cl molecule. The threshold energy $E_0 = 352 \pm 28$ kJ/mol exhibits an excess of 155 ± 30 kJ/mol over the reaction endothermicity of $\Delta H_0 = 197 \pm 10$ kJ/mol (Table 1). At higher energies, the decline in the ICl^- cross sections is related to the dissociation energy of $D(ICl^-) = 93 \pm 10$ kJ/mol (Table 1). Dissociation of ICl^- results predominantly in a contribution to the Cl^- cross sections from $ICl^- \rightarrow Cl^- + I$ because EA(Cl) = 3.613 eV is greater than EA(I) = 3.063 eV.[48] Figure 1 shows the Cl^- cross sections continue to rise after the initial decline in the ICl^- cross sections, supporting a source of Cl^- from front-side attack but by a dissociative mechanism rather than front-side nucleophilic displacement. This is supported by findings of Song and Hase,[49] who investigated the translation activation of the front-side transition state, **d**, for $Cl^- + CH_3Cl$ and concluded that the transition state cannot be attained by translational energy alone but instead requires preferential vibrational excitation of CH_3Cl.

4.3. $I^- + CH_3Br \rightarrow Br^- + [CH_3I]$. The ΔH_0 values listed in Table 2 show that the initial Br^- cross sections in the threshold region must be due to the formation of the $Br^- + CH_3I$ products. The PES for the S_N2 back-side attack mechanism is shown in Figure 4b. The energy of the front-side nucleophilic exchange transition state, **d**, is calculated by the CCSD(T)/LanL2DZ and CCSD(T)/SDD methods to be about 166 kJ/mol above the energy of the reactants and, therefore, too high to be responsible for the initial rise in the cross sections at 121 ± 10 kJ/mol. The reaction probably proceeds through the back-side attack route with an excess threshold energy of 94 ± 10 kJ/mol resulting from dynamical constrictions as discussed in section 4.5.[16] Above 2 eV, the initial rise in the Cl^- cross sections weakens but is followed by a second stronger rising feature above 4 eV. This weakening cross section behavior above 2 eV is probably related to competition from the bromine abstraction reaction and the second stronger rise at above 4 eV by a front-side attack mechanism and the dissociation of the IBr^- ion from reaction 2 as discussed next.

4.4. $I^- + CH_3Br \rightarrow IBr^- + [CH_3]$. Table 2 and Figure 2 show that the bromine abstraction reaction exhibits a threshold energy of $E_0 = 215 \pm 20$ kJ/mol. The only reaction that can proceed at these energies is formation of $IBr^- + CH_3$. The cross sections exhibit a steep initial rise followed by a less steep rise and a decline at energies above about 4 eV. The threshold energy of reaction 2 again exhibits an excess energy when compared to the reaction endothermicity, ΔH_0. The decline is most likely related to the dissociation energy of $D(IBr^-) = 106 \pm 10$ kJ/mol (Table 2). The dissociation of IBr^- results in a contribution to the Br^- cross sections from $IBr^- \rightarrow Br^- + I$; the electron affinities of Br and I are 3.363 and 3.063 eV, respectively.[48] Some I^- might also be formed via this dissociative mechanism but would not be observed against the I^- reactant ion background.

4.5. Dynamical Constrictions. Previously,[16,25] we observed similar excess threshold energies for the reactions of $Cl^- + CH_3F$ and $Cl^- + CH_3Cl$ and discussed three dynamic effects that can contribute to the observed high threshold energy: angular momentum conservation, orientational or steric constraints, and translational versus vibrational energy requirements. The following is a brief discussion of the dynamical constrictions which can effect the efficiency of translational-driven gas phase reactions. For a more detailed discussion, the reader is directed to our previous publications on the $Cl^- + CH_3F$ and $Cl^- + CH_3Cl$ reactions.[16,25]

Angular Momentum Barriers. Angular momentum conservation has been previously discussed as a dynamical impediment to translational activation of gas-phase S_N2.[13,16,25,50] High orbital angular momenta can be generated by collisions at a high translation energy and nonzero impact parameters. The angular momentum must be conserved as the system passes through the transition-state region. Because the moment of inertia at the tight transition state is smaller than that of the colliding reactants or the ion−dipole complexes, high rotational energies are required to conserve angular momentum, which in turn reduces the energy available along the reaction coordinate. Figure 4 illustrates the effective potential energy including the angular momentum term (centrifugal energy) at the S_N2 stationary points. The effective potential energy in the spherical approximation is given by eq 4,

$$V_{\text{eff}} = V + \frac{L^2}{2I} \tag{4}$$

where V is the potential energy, $L = \mu v b$ is the orbital angular momentum, μ is the reduced mass of reactants, v and $E = \mu v^2/2$ are the initial relative collision velocity and energy, b is the impact parameter, and I is the moment of inertia calculated from CCSD(T)/LanL2DZ rotational constants. Figure 4 shows that the angular momentum barrier at the S_N2 transition state becomes dominant for high values of Eb^2 for both reactions. At the observed threshold energies, V_{eff} is less than E_0 for impact parameters less than 4.0 and 4.7 Å for reaction 1 with CH_3Cl and CH_3Br, respectively. However, the cross sections near the threshold exhibited in Figures 1 and 2 are several orders of magnitude smaller than would be calculated from these limiting impact parameters.

The importance of angular momentum effects can be further investigated by classical PST, a form of microcanonical transition state theory that explicitly conserves total angular momentum.[38−40] The experimental results are compared to PST in Figures 1 and 2. In the PST model, the total angular momentum is approximated by the orbital angular momentum from the collision process and the phase space for the rotational degrees of freedom of the transition state is calculated classically using the spherical rotor approximation for nonlinear molecules. The PST cross sections include a convolution over the experimental energy distributions. The $I^-\cdots CH_3X$ ion−molecule complex is formed by capture over the centrifugal barrier of the long-range electrostatic ion−molecule potential, followed by statistical unimolecular decomposition of the complex either back to reactants via an orbiting transition state or to the products of either reaction 1or 2. For reaction 1, we calculated the cross sections for passage through the back-side S_N2 transition state **b** and the front-side nucleophilic displacement transition state **d**. For reaction 2, the cross sections are calculated using an orbiting transition state of the products because the PES exhibited in Figure 5a,b shows there are no barriers in excess of the energy of the products. PST provides an upper limit for

cross sections based on energy and angular momentum conservation. The molecular parameters used in calculating the PST cross sections are taken from experiments[33,48] and the CCSD(T)/LanL2DZ theoretical calculations. The PST cross sections for the back-side S_N2 reaction rise from a threshold equal to ΔH_0 (Tables 1 and 2) to a similar magnitude of the experimental cross sections. The front-side displacement reaction rises from the energy of the front-side displacement transition state relative to the reactants and also exhibits similar magnitude cross sections to the experiment. The PST cross sections for the halide abstraction reaction rise from a threshold equal to ΔH_0 but result with cross sections 10 times the magnitude of the experimental cross sections. Interestingly, PST predicts the crossing of the halogen abstraction cross sections over the nucleophilic displacement cross sections. The disagreement between PST and the experimental cross sections indicate that angular momentum barriers alone cannot account for the excess threshold energies and show that the reactions are direct and nonstatistical.

Orientational Constraints. Passage over the S_N2 central barrier in Figure 4 requires, at low energies, that the I^- be aligned for back-side attack along the CY bond axis. The height of the S_N2 barrier increases as the I−C−Y angle deviates from 180°.[16] The S_N2 reactions are likely to have a direct reaction mechanism already at the threshold collision energy because there is not enough time for reorientation during a collision event. Therefore, reaction 1 should have a strong orientation dependence. Orientational effects can explain a slow-rising cross section above the threshold,[51] but it cannot completely explain a large shift in the threshold energy. However, orientational effects are coupled to inefficient translational to vibrational energy transfer as discussed next.

Translational versus Vibrational Energy Activation. The PES in Figure 4 can be interpreted in terms of typical Polanyi behavior for an endoergic reaction with a late transition state.[52] The transition states of the S_N2 reactions are considered "late" as the C−Y bond is significantly stretched from the equilibrium distance of the free CH_3Y molecule.[16,53] For the reaction to proceed efficiently there is a need for vibrational energy in the C−Y stretching mode of CH_3Y. Hase et al.[4,21,22,54] have shown that the formation of the entrance complex is accompanied by poor energy coupling due to the short lifetime of less than 10 ps of the complex. This results in a high dissociation rate back to reactants. The direct dynamics and tight transition state of the S_N2 reactions restrict the coupling of translational and vibrational modes and result in inefficient activation of the reaction by translational energy. At higher energies, the orientational acceptance angle of the PES for back-side attack opens up and the dynamic constraints on translational energy activation become less severe, allowing the reaction to proceed. We hypothesize that this effect is the most important, which could be studied further by theoretical reaction dynamics or vibrationally state selective experiments.

5. Conclusions

Two competing reactions, nucleophilic displacement and halogen abstraction, have been detected by guided ion beam techniques from the reactions of $I^- + CH_3Cl$ and $I^- + CH_3Br$. Both reactions have excess threshold energies when compared to the reaction endothermicities. The observed elevated threshold energies can be explained by a combination of angular momentum barriers, orientational effects, and the inefficiency of activation by translational energy. For reaction 2, a "competitive shift"[55] from the lower-energy nucleophilic displacement reaction may also be an impediment. The experimental and theoretical results support the view that at the threshold nucleophilic displacement occurs predominantly through the S_N2 back-side attack mechanism with inversion of the methyl group. At higher energies the front-side halogen abstraction reaction proceeds, indicating a front-side attack. Nucleophilic displacement may occur at these higher energies through a front-side attack transition state, although there is more direct evidence for a reaction occurring via the halogen abstraction reaction and subsequent dissociation of the IY^- molecule.

We have previously observed excess translational threshold energies for endoergic anion−molecule reactions where there is no actual potential energy barrier in excess of the reaction endoergicity.[16,25,56] Without exception, these are associated with the presence of a tight transition state along the reaction path, as at the central barrier for the $X^- + CH_3Y$ S_N2 reactions.[16,25] The excess threshold energies can be huge for endoergic S_N2 reactions: 52 ± 16 kJ/mol for (X, Y) = (Cl, F),[16] 77 ± 31 kJ/mol for (I, Cl), and 94 ± 10 kJ/mol for (I, Br). This last case has an apparent threshold energy that is 4.7 times the thermochemical endoergicity! Such high effective thresholds cannot be explained merely by the low density of states and angular momentum constrictions at the tight transition state. PST, which quantitatively accounts for those effects, predicts cross sections that rise close to the thermochemical threshold energy. Therefore, these reactions are certainly nonstatistical. A major dynamic constraint, consistent with experimental[16,25,56] and theoretical[57,58] evidence, is the requirement of translational-to-vibrational energy transfer for reaction to occur. The S_N2 central barriers are characterized as "late" transition states, especially for the endothermic reactions, that is, the C−Y bond is considerably stretched at the transition state. According to Polanyi rules,[52,59] that means that translational energy is inefficient in promoting the reaction. Furthermore, the tight orientational constraints of the S_N2 transition states for back-side attack restricts the reactions very closely to a pseudo-collinear path. That in turn reinforces the inefficiency of translational energy promotion, because the reaction path must navigate a tight corner in the mass-skewed coordinates on the pseudo-collinear PES. The mass-skew angles are 51, 38, and 30° for the (Cl, F), (I, Cl), and (I, Br) reactions, respectively, that is, the tighter the angle, the higher the observed excess energy threshold. Thus, the combination of the late transition states, orientational restrictions, and kinematic mass effects all conspire to give high excess threshold energies for endoergic S_N2 reactions.

References and Notes

(1) Laerdahl, J. K.; Uggerud, E. *Int. J. Mass Spectrom.* **2002**, *214*, 277.
(2) Gronert, S. *Chem. Rev.* **2001**, *101*, 329.
(3) Chabinyc, M. L.; Craig, S. L.; Regan, C. K.; Brauman, J. I. *Science* **1998**, *279*, 1882.
(4) Hase, W. L. *Science* **1994**, *266*, 998.
(5) Shaik, S. S.; Schlegel, H. B.; Wolfe, S. *Theoretical Aspects of Physical Organic Chemistry: The S_N2 Mechanism*; John Wiley and Sons: New York, 1992.
(6) Olmstead, W. N.; Brauman, J. I. *J. Am. Chem. Soc.* **1977**, *99*, 4219.
(7) Dodd, J. A.; Brauman, J. I. *J. Phys. Chem.* **1986**, *90*, 3559.
(8) Brauman, J. I. *J. Mass Spectrom.* **1995**, *30*, 1649.
(9) Levine, R. D.; Bernstein, R. B. *J. Phys. Chem.* **1988**, *92*, 6954.
(10) Wang, H.; Peslherbe, G. H.; Hase, W. L. *J. Am. Chem. Soc.* **1994**, *116*, 9644.
(11) Peslherbe, G. H.; Wang, H.; Hase, W. L. *J. Am. Chem. Soc.* **1996**, *118*, 2257.
(12) Su, T.; Morris, R. A.; Viggiano, A. A.; Paulson, J. F. *J. Phys. Chem.* **1990**, *94*, 8426.
(13) Wang, H.; Hase, W. L. *J. Am. Chem. Soc.* **1997**, *119*, 3093.
(14) Su, T.; Wang, H.; Hase, W. L. *J. Phys. Chem. A* **1998**, *102*, 9819.
(15) Schmatz, S.; Clary, D. C. *J. Chem. Phys.* **1999**, *110*, 9483.

(16) Angel, L. A.; Garcia, S. P.; Ervin, K. M. *J. Am. Chem. Soc.* **2002**, *124*, 336.
(17) Graul, S. T.; Bowers, M. T. *J. Am. Chem. Soc.* **1991**, *113*, 9696.
(18) Graul, S. T.; Bowers, M. T. *J. Am. Chem. Soc.* **1994**, *116*, 3875.
(19) Viggiano, A. A.; Morris, R. A.; Paschkewitz, J. S.; Paulson, J. F. *J. Am. Chem. Soc.* **1992**, *114*, 10477.
(20) Wang, H.; Hase, W. L. *J. Am. Chem. Soc.* **1995**, *117*, 9347.
(21) Wang, H.; Hase, W. L. *Chem. Phys.* **1996**, *212*, 247.
(22) Wang, H.; Goldfield, E. M.; Hase, W. L. *J. Chem. Soc., Faraday Trans.* **1997**, *93*, 737.
(23) Tonner, D. S.; McMahon, T. B. *J. Am. Chem. Soc.* **2000**, *122*, 8783.
(24) Cyr, D. A.; Scarton, M. G.; Wiberg, K. B.; Johnson, M. A.; Nonose, S.; Hirokawa, J.; Tanaka, H.; Kondow, T.; Morris, R. A.; Viggiano, A. A. *J. Am. Chem. Soc.* **1995**, *117*, 1828.
(25) DeTuri, V. F.; Hintz, P. A.; Ervin, K. M. *J. Phys. Chem. A* **1997**, *101*, 5969.
(26) Angel, L. A.; Ervin, K. M. *J. Phys. Chem. A* **2001**, *105*, 4042.
(27) Angel, L. A.; Ervin, K. M. *J. Am. Chem. Soc.* **2003**, *125*, 1014.
(28) Zellermann, G.; Vietzke, E. *Radiochim. Acta* **1990**, *50*, 107.
(29) Ervin, K. M.; Armentrout, P. B. *J. Chem. Phys.* **1985**, *83*, 166.
(30) Armentrout, P. B. *Int. J. Mass Spectrom.* **2000**, *200*, 219.
(31) Schultz, R. H.; Crellin, K. C.; Armentrout, P. B. *J. Am. Chem. Soc.* **1991**, *113*, 8590.
(32) Dalleska, N. F.; Honma, K.; Sunderlin, L. S.; Armentrout, P. B. *J. Am. Chem. Soc.* **1994**, *116*, 3519.
(33) Herzberg, G. *Molecular Spectra and Molecular Structure II. Infrared and Raman Spectra of Polyatomic Molecules*; Van Nostrand Reinhold: New York, 1945.
(34) Chantry, P. J. *J. Chem. Phys.* **1971**, *55*, 2746.
(35) Lifshitz, C.; Wu, R.; Tiernan, T.; Terwilleger, D. *J. Chem. Phys.* **1978**, *68*, 247.
(36) Taylor, B. N.; Kuyatt, C.; NIST Technical Note 1297; National Institute of Standards and Technology: Washington, DC, 1994.
(37) Armentrout, P. B.; Ervin, K. M.; *CRUNCH*, Fortran program, version 5.0; 2004.
(38) Pechukas, P.; Light, J. C. *J. Chem. Phys.* **1965**, *42*, 3281.
(39) Chesnavich, W. J.; Bowers, M. T. *J. Chem. Phys.* **1977**, *66*, 2306.
(40) Aue, D. H.; Bowers, M. T. In *Gas-Phase Ion Chemistry*; Bowers, M. T., Ed.; Academic: New York, 1979; p 1.
(41) Frisch, M. J.; Trucks, G. W.; Schlegel, H. B.; Scuseria, G. E.; Robb, M. A.; Cheeseman, J. R.; Zakrzewski, V. G.; Montgomery, J. A., Jr.; Stratmann, R. E.; Burant, J. C.; Dapprich, S.; Millam, J. M.; Daniels, A. D.; Kudin, K. N.; Strain, M. C.; Farkas, O.; Tomasi, J.; Barone, V.; Cossi, M.; Cammi, R.; Mennucci, B.; Pomelli, C.; Adamo, C.; Clifford, S.; Ochterski, J.; Petersson, G. A.; Ayala, P. Y.; Cui, Q.; Morokuma, K.; Malick, D. K.; Rabuck, A. D.; Raghavachari, K.; Foresman, J. B.; Cioslowski, J.; Ortiz, J. V.; Stefanov, B. B.; Liu, G.; Liashenko, A.; Piskorz, P.; Komaromi, I.; Gomperts, R.; Martin, R. L.; Fox, D. J.; Keith, T.; Al-Laham, M. A.; Peng, C. Y.; Nanayakkara, A.; Gonzalez, C.; Challacombe, M.; Gill, P. M. W.; Johnson, B. G.; Chen, W.; Wong, M. W.; Andres, J. L.; Head-Gordon, M.; Replogle, E. S.; Pople, J. A. *Gaussian 98*, revision A.7; Gaussian, Inc.: Pittsburgh, PA, 1998.
(42) Gurvich, L. V.; Veyts, I. V.; Alcock, C. B. *Thermodynamic Properties of Individual Substances*, 4th ed.; Hemisphere Publishing Corp.: New York, 1989; Vol. 1 (Elements O, H (D, T), F, Cl, Br, I, He, Ne, Ar, Kr, Xe, Rn, S, N, P and Their Compounds), Parts 1−2.
(43) Gurvich, L. V.; Veyts, I. V.; Alcock, C. B. *Thermodynamic Properties of Individual Substances*, 4th ed.; Hemisphere: New York, 1991; Vol. 2 (Elements C, Si, Ge, Sn, Pb, and Their Compounds), Parts 1−2.
(44) Dunning, T. H. J.; Hay, P. J. *Modern Theoretical Chemistry*; Schaefer, H. F., Ed.; Plenum: New York, 1976; Vol. 3, p 1.
(45) Wadt, W. R.; Hay, P. J. *J. Chem. Phys.* **1985**, *82*, 284.
(46) Igel-Mann, G.; Stoll, H.; Preuss, H. *Mol. Phys.* **1988**, *65*, 1321.
(47) Glukhovtsev, M. N.; Pross, A.; Radom, L. *J. Am. Chem. Soc.* **1996**, *118*, 6273.
(48) *CRC Handbook of Chemistry and Physics*, 83rd ed.; Linde, D. R., Ed.; CRC Press: Boca Raton, FL, 2002.
(49) Song, K.; Hase, W. L. *J. Chem. Phys.* **1999**, *110*, 6198.
(50) Mann, D. J.; Hase, W. L. *J. Phys. Chem. A* **1998**, *102*, 6208.
(51) Ervin, K. M. *Int. J. Mass Spectrom.* **1999**, *185/186/187*, 343.
(52) Polanyi, J. C.; Wong, W. H. *J. Chem. Phys.* **1969**, *51*, 1439.
(53) Vande Linde, S. R.; Hase, W. L. *J. Phys. Chem.* **1990**, *94*, 2778.
(54) Cho, Y. J.; Vande Linde, S. R.; Zhu, L.; Hase, W. L. *J. Chem. Phys.* **1992**, *96*, 8275.
(55) Chupka, W. A. *J. Chem. Phys.* **1959**, *30*, 191.
(56) Angel, L.; Dogbevia, M.; Rempala, K.; Ervin, K. *J. Chem. Phys.* **2003**, *119*, 8996.
(57) Su, T.; Wang, H.; Hase, W. L. *J. Phys. Chem. A* **1998**, *102*, 9819.
(58) Vande Linde, S. R.; Hase, W. L. *J. Am. Chem. Soc.* **1989**, *111*, 2349.
(59) Polanyi, J. C. *Acc. Chem. Res.* **1972**, *5*, 161.
(60) *NIST Chemistry WebBook, NIST Standard Reference Database Number 69*; Mallard, W. G., Linstrom, P. J., Eds.; National Institute of Standards and Technology: Gaithersburg, MD, 2000.